SLAC-PUB-188

ASYMMETRIC MU-PAIR PHOTOPRODUCTION AND QUANTUM ELECTRODYNAMICS AT SMALL DISTANCES*

R. G. Parsons†

Stanford Linear Accelerator Center
Stanford University, Stanford, California

(Submitted to Physical Review)

*Work supported by the U. S. Atomic Energy Commission.

†Part of a dissertation submitted in partial fulfillment of the requirements of a Ph.D. degree to the Department of Physics, Stanford University, Stanford, California. Further calculational details will be found in the dissertation.

+(2)

ABSTRACT

A sensitive test of the theory of quantum electrodynamics as applied to muons is analyzed in this paper. The test consists of photoproducing mu-pairs in hydrogen such that the negative muon is produced at small angles with respect to the incident photon and with nearly all of the available energy. The positive muon and the recoil proton are not detected. The cross section is calculated from the Bethe-Heitler amplitude treating proton recoil exactly. The effect of proton structure is analyzed in terms of the two form factors measured by elastic electron-proton scattering. These form factors are approximated by a power series in the invariant four momentum q^2 transferred to the nucleus.

Radiative corrections appropriate for the experimental resolution are calculated and are shown to reduce the Bethe-Heitler cross section by about five per cent. The cross section for muon pairs from the decay of known heavy vector resonances is found to be negligible. The flux of negative muons from the decay of a photoproduced π^- is calculated and is shown to be a limiting factor in choosing the energy resolution of an experiment.

I. INTRODUCTION

In the past few years, the results of several experiments have cast doubt upon the validity of quantum electrodynamics at small distances.[1,2] A new test of quantum electrodynamics as applied to muons has been proposed by Drell[3] in which muon pairs are photoproduced in an extremely asymmetric kinematic condition. In this paper, a detailed analysis of this proposed experiment is made.

In the asymmetric kinematic configuration, the negative muon is produced in hydrogen at small angles with respect to the incident photon and with almost all of the available energy. The positive muon and the recoil proton are not observed. This arrangement is advantageous to electron linear accelerators since these machines produce intense beams of electrons and photons concentrated in very short pulses. This makes coincidence experiments much more difficult than single-particle counting experiments. We choose to detect the negative muon since, in the absence of neutrons in the target, the threshold for producing a high energy μ^- by the reaction

$$\gamma + p \rightarrow \pi^- + \pi^+ + p$$
$$\qquad\quad \hookrightarrow \mu^- + \bar{\nu}_\mu$$

is approximately 40 MeV below the threshold for the reaction $\gamma + p \rightarrow \mu^- + \mu^+ + p$. Thus, if the energy resolution of the detection apparatus is restricted to a 40 MeV region below the μ-pair threshold, any μ^- detected is guaranteed to be one member of a pair. The

production of a single μ^- or π^- from hydrogen is excluded by charge conservation. If the energy resolution of the experiment is larger than 40 MeV, a correction must be made to the observed counting rate to allow for muons from pion decay.

The prediction of quantum electrodynamics for the muon pair photoproduction cross section is calculated in the usual way from the matrix elements corresponding to the two Feynman diagrams in Fig. 1. This experiment probes quantum electrodynamics at small distances since the virtual muon in Fig. 1(b) is forced to be far off its mass shell. If the undetected μ^+ is non-relativistic, the mass of this virtual muon is $\approx (2mk)^{1/2}$. The virtual muon in Fig. 1(a) is much closer to the mass shell with

$$(k - p_-)^2 - m^2 \approx - m^2 (1 + \theta_-^2 k^2/m^2) \quad .$$

However, in transverse gauge in the laboratory, both diagrams are found to give approximately equal contributions. Thus, if the muon propagator differs from that predicted by the present theory of quantum electrodynamics for muons far off their mass shell, the experimental cross section will be different from the cross section calculated in this paper.

The effect of proton structure in first Born approximation can be completely and unambiguously accounted for in terms of the two invariant form factors measured in elastic electron-proton scattering, G_E and G_M, which depend only on the invariant momentum

transfer q^2. This is a consequence of the vector nature of the exchanged virtual photon and of electromagnetic current conservation. Besides approximating the form factors by a power series in q^2, no other approximations are made in calculating the pair production cross section to lowest order in α. The method of integration over the unobserved muon and proton is such that the expansion of the form factors can be made as accurate as desired by adding higher powers of q^2.

The expression for the pair production cross section in lowest order in α is derived in Section II. In Section III, radiative corrections appropriate for the proposed experimental situation are calculated, keeping terms of order $\ell n\,(\omega_-/m)$ relative to unity. These corrections reduce the cross section by ≈ 5 per cent for photon energies of ≈ 15 GeV and an evergy resolution of ≈ 200 MeV. In Section IV, an analysis is made of the contribution of virtual Compton terms such as the photoproduction of vector resonances with their subsequent decay into a muon pair. In Section V, we estimate the flux of negative pions photoproduced in the target. These particles can produce a spurious background of muons, and their presence imposes an upper limit on the energy resolution of an experiment.

II. DETAILS OF THE PAIR PRODUCTION CALCULATION

The general formula for muon pair production in the first Born approximation has been derived by Drell and Walecka.[4] Their formula includes all nuclear effects. The set of six invariants which were chosen for that paper were not convenient for the asymmetric kinematic configuration and a new set shown below was chosen for this paper. If hydrogen is used as the nuclear target, there are only five independent invariants since the invariant mass of the final nuclear state is the same as that of the initial nuclear state.

Table I defines all symbols used in this paper. We chose the five independent scalars to be

$$\begin{aligned} y_1 &= 2k\cdot p_- \ , \\ y_2 &= 2k\cdot q \ , \\ y_3 &= 2k\cdot P \ , \\ y_4 &= 2P\cdot z \ , \\ y_5 &= q^2 \ , \end{aligned} \tag{1}$$

where $z = p_- - k$. In addition we define $x_2 = y_2 - y_1 = 2k\cdot p_+$.

The prediction of quantum electrodynamics for the cross section for muon pair production can be evaluated by standard techniques using the two Feynman diagrams of Fig. 1. One finds

$$d\sigma = \frac{\alpha^3}{\pi^2} \frac{d^3p_-}{2\omega_-} \frac{d^3p_+}{2\omega_+} \frac{d^3P'}{E'} \frac{1}{q^4} \frac{1}{k\cdot P} \delta^4(k+P-P'-p_+-p_-)\, W_{\mu\nu}\, M^{\mu\nu} \ , \tag{2}$$

where

$$W_{\mu\nu} M^{\mu\nu} = \frac{4}{y_1} W_1(y_5) \left\{ - x_2 + \left[f_1 y_5 + f_2 \right] \right.$$

$$+ \frac{1}{x_2} \left[- 2y_5^2 + f_3 y_5 + f_4 \right]$$

$$\left. + \frac{1}{x_2^2} \left[f_5 y_5 + f_6 \right] \right\}$$

$$+ \frac{4}{y_1} W_2(y_5) \left\{ - \frac{1}{2} x_2 + \left[f_7 y_5 + f_8 \right] \right. \tag{3}$$

$$+ \frac{1}{x_2} \left[f_9 y_5^2 + f_{10} y_5 + f_{11} \right]$$

$$\left. + \frac{1}{x_2^2} \left[f_{12} y_5 + f_{13} \right] \right\} \quad ,$$

and where

$$W_1(q^2) = \frac{q^2}{4} G_M^2(q^2) \quad , \tag{4}$$

$$W_2(q^2) = \frac{M^2}{1 - q^2/4M^2} \left[G_E^2(q^2) - \frac{q^2}{4M^2} G_M^2(q^2) \right] \quad . \tag{5}$$

G_E and G_M are the usual electric and magnetic form factors for the proton. In order to do the final phase space integrals for the positive muon and the recoil proton in closed form, we approximate W_1 and W_2 as follows :

$$W_1(q^2) \approx q^2 (\tfrac{1}{4} \mu^2 + B_1 q^2 + C_1 q^4) \tag{6}$$

$$W_2(q^2) \approx M^2 (1 + B_2 q^2 + C_2 q^4) \quad . \tag{7}$$

The constants $f_{1\cdots13}$ are functions of the fixed kinematic variables and are listed below in units of the muon mass (m = 1).

$$
\begin{aligned}
f_1 &= 2\left(\frac{1}{y_1} - 1\right) \\
f_2 &= 4f_1 + 4 \\
f_3 &= -2y_1 \\
f_4 &= 8\left(1 - \tfrac{1}{2}\, y_1 - \tfrac{1}{8}\, y_1^{\,2}\right) \\
f_5 &= -f_3 \\
f_6 &= 2f_5 \\
f_7 &= \frac{1}{y_1}\left(1 - \frac{2z_o}{M}\right) - 1 + \frac{1}{M}\left(k_o + z_o\right) \\
f_8 &= \frac{4z_o^{\,2}}{y_1} \\
f_9 &= -1 + \frac{1}{M}\left(\frac{y_1}{2M} + 2z_o + k_o\right) \\
f_{10} &= 2\left(-\tfrac{1}{2}\, y_1\left(1 + \frac{z_o}{M}\right) + 1 - 2z_o^{\,2} - \left(k_o + \frac{1}{M}\right)\left(k_o + 2z_o\right)\right) \\
f_{11} &= -\tfrac{1}{2}\, y_1^{\,2} + 8z_o\left(k_o + z_o\right) \\
f_{12} &= y_1\left(1 - \frac{2}{M}\left(k_o + z_o\right)\right) \\
f_{13} &= 4y_1\left(k_o + z_o\right)^2
\end{aligned}
\tag{8}
$$

The positive muon and the recoil proton are not observed so the phase space integrals for p_+ and P' must be carried out. Since the proton form factors are functions only of q^2, it is advantageous to change integration variables so that the invariant q^2 becomes one of the new integration variables. In this way the double differential cross section $d^2\sigma/d\Omega_- \, d\omega_-$ can be written as an indefinite integral in q^2. The value of the cross section is then obtained by evaluating the indefinite integral at the kinematical maximum and minimum of q^2 as determined from k_o, ω_-, and θ_-. Approximating the "form factors" by a power series in q^2 permits one to do the integrals in closed form.

In terms of the new integration variables, the phase space integrals may be written as

$$\int \frac{d^3p_+}{2\omega_+} \frac{d^3P'}{E'} \delta^4(k+P-P'-p_+-p_-) = \int dq^2 \int_0^{2\pi} d\varphi_q \frac{1}{4M|\underset{\sim}{z}|} \quad , \qquad (9)$$

where φ_q is the azimuthal angle of $\underset{\sim}{q}$ with respect to $\underset{\sim}{z} = \underset{\sim}{p}_- - \underset{\sim}{k}$. The invariant $x_2 = y_2 - y_1$ is the only invariant which depends on φ_q and is of the form $x_2 = d - e \cos \varphi_q$ where d and e are functions of q^2.

Finally we may write (for the laboratory system)

$$\frac{d^2\sigma}{d\Omega_- \, d\omega_-} = \frac{\alpha^3}{\pi^2} \frac{1}{k_o M} \frac{1}{4M|\underset{\sim}{z}|} \frac{|\underset{\sim}{p}_-|}{2} 2\pi \left[\Sigma\left(q^2_{max}\right) - \Sigma\left(q^2_{min}\right)\right] \quad , \qquad (10)$$

where

$$\Sigma(q^2) \equiv \int dq^2 \int_0^{2\pi} \frac{d\varphi_q}{2\pi} \frac{1}{q^4} \left(W_{\mu\nu} M^{\mu\nu}\right) \quad .$$

The indefinite integral $\Sigma(x)$ has been evaluated and is shown below.

$$\Sigma(x) = \frac{\mu^2}{y_1}\left\{(f_1 - g)\,x + (f_2 - h)\,\ln x - 2I_1 + f_3 I_0 + f_4 I_{-1} + f_5 J_0 + f_6 J_{-1}\right\}$$

$$+ \frac{4B_1}{y_1}\left\{(f_1 - g)\,\frac{x^2}{2} + (f_2 - h)\,x - 2I_2 + f_3 I_1 + f_4 I_0 + f_5 J_1 + f_6 J_0\right\}$$

$$+ \frac{4C_1}{y_1}\left\{(f_1 - g)\,\frac{x^3}{3} + (f_2 - h)\,\frac{x^2}{2} - 2I_3 + f_3 I_2 + f_4 I_1 + f_5 J_2 + f_6 J_1\right\} \qquad (11)$$

$$+ \frac{4M^2}{y_1}\left\{(f_7 - \tfrac{1}{2}g)\,\ln x - (f_8 - \tfrac{1}{2}h)\,\frac{1}{x} + f_9 I_0 + f_{10} I_{-1} + f_{11} I_{-2} + f_{12} J_{-1} + f_{13} J_{-2}\right\}$$

$$+ \frac{4M^2 B_2}{y_1}\left\{(f_7 - \tfrac{1}{2}g)\,x + (f_8 - \tfrac{1}{2}h)\,\ln x + f_9 I_1 + f_{10} I_0 + f_{11} I_{-1} + f_{12} J_0 + f_{13} J_{-1}\right\}$$

$$+ \frac{4M^2 C_2}{y_1}\left\{(f_7 - \tfrac{1}{2}g)\,\frac{x^2}{2} + (f_8 - \tfrac{1}{2}h)\,x + f_9 I_2 + f_{10} I_1 + f_{11} I_0 + f_{12} J_1 + f_{13} J_0\right\},$$

where

$$d = gq^2 + h = 2k_o \left[\frac{q^2}{2M} - \frac{y_1}{2k_o} - \left(\frac{q^4}{4M^2} - q^2 \right)^{1/2} \cos\theta_k \cos\theta_q \right] ,$$

$$e = 2k_o \left[\left(\frac{q^4}{4M^2} - q^2 \right)^{1/2} \sin\theta_k \sin\theta_q \right] ,$$

$$\left(\frac{q^4}{4M^2} - q^2 \right)^{1/2} \cos\theta_q = \frac{1 - q^2 - z^2 + q^2 \left(\frac{P \cdot z}{M^2} \right)}{2|z|} ,$$

$$(d^2 - e^2)^{1/2} \equiv (a\, q^4 + b\, q^2 + c)^{1/2} ,$$

$$I_n \equiv \int \frac{x^n\, dx}{(a\, x^2 + b\, x + c)^{1/2}} ,$$

$$J_n \equiv \int \frac{(g\, x + h)\, x^n\, dx}{(a\, x^2 + b\, x + c)^{3/2}} .$$

The values of q^2_{max} and q^2_{min} are respectively the two roots of the following quadratic equation in q^2:

$$q^4 \left(- \frac{z^2}{M^2} - 1 + \frac{2z_o}{M} \right) + q^2 \left(2 \left(1 - \frac{z_o}{M} \right) (m^2 - z^2) + 4 \left(z^2 - z_o^2 \right) \right) - (m^2 - z^2)^2 = 0 . \tag{12}$$

If necessary, one may easily extend the definition of $\Sigma(x)$ to include higher terms in the expansion of W_1 and W_2. This expansion is the only approximation made in calculating $d^2\sigma/d\Omega_-\, d\omega_-$ to the lowest order in α.

A computer program has been written in SUBALGOL for the Stanford IBM 7090 to tabulate $d^2\sigma/d\Omega_- \, d\omega_-$ for arbitrary values of k_o, ω_-, and θ_- .

III. RADIATIVE CORRECTIONS

In this section, we calculate the radiative corrections to σ_{B-H} due to both real and virtual photons. These corrections fall into two categories: and infrared term containing a resolution logarithm $\ell n(\omega_-/\Delta E)$ and a remainder term not depending on the resolution logarithm. The infrared term consists of a factor multiplying the Bethe-Heitler matrix element. In this term, proton recoil and proton structure corrections are retained. The remainder terms are small (of the order of one per cent) and we have neglected proton structure and proton recoil in these terms.

The calculation was divided into three parts. In (A), following Yennie, Frautschi, and Suura,[5] we isolate that part of both the real and virtual radiative corrections which contains an infrared divergence. The sum of these two parts is independent of the "photon mass" and is of order $\alpha\, \ell n(\omega_-/m)\ell n(\omega_-/\Delta E)\sigma_{B-H}$. In (B) the remainder of the virtual photon terms are calculated, and in (C) the remainder of the real photon terms are calculated.

A. Infrared Terms

Of the fourteen virtual photon diagrams in Fig. 2, only diagrams 5V, 6V, 7V, 8V, 11V, and 12V contain infrared divergences. The matrix elements corresponding to diagrams 11V and 12V may be written as

$$M_{11V} + M_{12V} = \left(M_{11V} + M_{12V}\right)_{IR} + \left(M_{11V} + M_{12V}\right)_{rem} ,$$

where

$$\left(M_{11V} + M_{12V}\right)_{IR} = \frac{ie^4}{(2\pi)^4}\frac{1}{q^2}\int \frac{d^4\ell}{\ell^2 - \lambda^2 + i\epsilon} \times$$

$$\times \left(\frac{(2p_- - \ell)\cdot(-2p_+ - \ell)}{(\ell^2 - 2p_-\cdot\ell)(\ell^2 + 2p_+\cdot\ell)}\right)\bar{u}(p_-)\left\{\epsilon\cdot\gamma\,\frac{1}{p_-\cdot\gamma - k\cdot\gamma - m}\,a\cdot\gamma\right. \tag{13}$$

$$\left. + a\cdot\gamma\,\frac{1}{-p_+\cdot\gamma + k\cdot\gamma - m}\,\epsilon\cdot\gamma\right\} v(p_+) \quad .$$

The remainder term $\left(M_{11V} + M_{12V}\right)_{rem}$ is not infrared divergent. If we now examine the expression

$$\alpha_B \equiv \frac{i\alpha}{8\pi^3}\int \frac{d^4\ell}{\ell^2 - \lambda^2 + i\epsilon}\left(\frac{(2p_- - \ell)_\mu}{(\ell^2 - 2p_-\cdot\ell)} + \frac{(2p_+ + \ell)_\mu}{(\ell^2 + 2p_+\cdot\ell)}\right)^2 , \tag{14}$$

we see that one can write

$$\frac{1}{2}\left(M_{5V} + M_{6V} + M_{7V} + M_{8V}\right) + \left(M_{11V} + M_{12V}\right)_{IR} = \alpha_B\, M_{B\text{-}H} \quad ,$$

where $M_{B\text{-}H}$ is the matrix element for the two Bethe-Heitler diagrams in Fig. 1.

$$M_{B\text{-}H} = \frac{-4\pi\alpha}{q^2}\,\bar{u}(p_-)\left\{\epsilon\cdot\gamma\,\frac{1}{p_-\cdot\gamma - k\cdot\gamma - m}\,a\cdot\gamma\right. \tag{15}$$

$$\left. + a\cdot\gamma\,\frac{1}{-p_+\cdot\gamma + k\cdot\gamma - m}\,\epsilon\cdot\gamma\right\} v(p_+)$$

The integral α_B is not ultraviolet divergent. Since $(M_{5V} + M_{6V} + M_{7V} + M_{8V})$ is ultraviolet divergent and $(M_{11V} + M_{12V})$ is not ultraviolet divergent, the term $\left(M_{11V} + M_{12V}\right)_{rem}$ must now contain the ultraviolet divergence necessary to cancel the divergence from diagrams 1V, 2V, 3V, 4V, 9V, and 10V. We shall later see explicitly

that this is true.

Of the six real photon diagrams in Fig. 3, only diagrams 1R, 3R, 4R, and 6R contain infrared divergences. As in the virtual photon case, we may write

$$(M_{1R} + M_{3R} + M_{4R} + M_{6R}) = \left(M_{1R} + M_{3R} + M_{4R} + M_{6R}\right)_{IR} + \left(M_{1R} + M_{3R} + M_{4R} + M_{6R}\right)_{rem} ,$$

where

$$\left(M_{1R} + M_{3R} + M_{4R} + M_{6R}\right)_{IR} =$$

$$= -\frac{e^3}{q^2}\left(\frac{p_-\cdot\eta}{p_-\cdot\ell} - \frac{p_+\cdot\eta}{p_+\cdot\ell}\right)\bar{u}(p_-)\left\{\epsilon\cdot\gamma\,\frac{1}{p_-\cdot\gamma - k\cdot\gamma - m}\,a\cdot\gamma + a\cdot\gamma\,\frac{1}{-p_+\cdot\gamma + k\cdot\gamma - m}\,\epsilon\cdot\gamma\right\} v(p_+) \qquad (16)$$

$$= e\left(\frac{p_-\cdot\eta}{p_-\cdot\ell} - \frac{p_+\cdot\eta}{p_+\cdot\ell}\right) M_{B\text{-}H} \ .$$

This term is gauge invariant in both photons and η is the polarization four vector of the soft photon in the final state.

The contribution of the real photon infrared terms to the cross section is found by squaring the matrix element and integrating over the appropriate final phase space. If we cut off the phase space integral for ℓ at $\ell_{max} = \Delta E$ and sum over the polarizations of the final state photon using $\sum_{pol} \eta_\nu \eta_\mu = -g_{\nu\mu}$, we get

$$\frac{1}{(2\pi)^3}\,\frac{1}{2}\int_0^{\Delta E} \frac{d^3\ell}{\left(\ell^2 + \lambda^2\right)^{\frac{1}{2}}} \sum_{pol}\left|\left(M_{1R} + M_{3R} + M_{4R} + M_{6R}\right)_{IR}\right|^2 \equiv 2\alpha\tilde{B}\left|M_{B\text{-}H}\right|^2 , \qquad (17)$$

where

$$\tilde{B} = \frac{-1}{8\pi^2}\int_0^{\Delta E} \frac{d^3\ell}{\left(\ell^2 + \lambda^2\right)^{\frac{1}{2}}}\left(\frac{p_-^\mu}{p_-\cdot\ell} - \frac{p_+^\mu}{p_+\cdot\ell}\right)^2 \quad . \tag{18}$$

The contribution of the virtual photon infrared term to the cross section is given by $2\alpha B\left|M_{B\text{-}H}\right|^2$. Adding the contribution from both the real and virtual infrared terms, we get a correction of

$$\sigma(\text{infrared}) = 2\alpha(\tilde{B} + \text{Re } B)\sigma_{B\text{-}H} \quad .$$

This quantity is independent of the photon mass λ and is given by[5]

$$\sigma(\text{infrared}) \approx \frac{\alpha}{\pi}\left[\left(\ell n\left(\frac{2p_+\cdot p_-}{m^2}\right) - 1\right)\ell n\left(\frac{\Delta E^2}{\omega_+\omega_-}\right) + \frac{1}{2}\ell n\left(\frac{2p_+\cdot p_-}{m^2}\right)\right]\sigma_{B\text{-}H} \quad . \tag{19}$$

This formula contains only the leading logarithmic terms under the condition $2p_+\cdot p_- \gg m^2$.

B. Virtual Photon Terms

The remaining virtual photon matrix elements were evaluated, keeping only those terms which contributed to order $\alpha\,\ell n(\omega_-/m)\sigma_{B\text{-}H}$. The matrix elements M_{9V}, M_{10V}, M_{13V}, and M_{14V} were calculated separately; M_{1V}, M_{3V}, and $\left(M_{11V}\right)_{rem}$ were calculated together over a common denominator as were M_{2V}, M_{4V}, and $\left(M_{12V}\right)_{rem}$. Diagrams 5V, 6V, 7V, and 8V were considered in part A of this section. The matrix elements listed below were evaluated assuming

$$2k\cdot p_+ \approx 2p_+\cdot p_- \gg -q^2 \gg 2k\cdot p_- \approx m^2 \quad .$$

The divergent integrals were evaluated using a large cutoff mass Λ on the photon propagator.

$$M_{1V} + M_{3V} + \left(M_{11V}\right)_{rem} =$$

$$= -\frac{\alpha^2}{q^2} \ln \frac{\Lambda^2}{m^2} \bar{u}(p_-) \left\{ a\cdot\gamma \frac{1}{-p_+\cdot\gamma + k\cdot\gamma - m} \epsilon\cdot\gamma \right\} v(p_+)$$

$$+ \frac{\alpha^2}{q^2} \bar{u}(p_-) \left\{ \frac{a\cdot\gamma\ k\cdot\gamma\ \epsilon\cdot\gamma}{(-2k\cdot p_+)} \left[\left(1 - \frac{3(2p_+\cdot p_-)}{(2k\cdot p_+)} + \frac{1}{2} \ln \left(\frac{-q^2}{m^2} \right) \right) \ln \left(\frac{2p_+\cdot p_-}{m^2} \right) \right] \right.$$

$$\left. + \frac{a\cdot\gamma\ p_-\cdot\gamma\ \epsilon\cdot\gamma}{(-2k\cdot p_+)} \left[\frac{1}{2} \ln \left(\frac{2k\cdot p_+}{m^2} \right) - \frac{1}{2} \left(\ln \left(\frac{-q^2}{m^2} \right) + 1 \right) \ln \left(\frac{2p_+\cdot p_-}{m^2} \right) \right] \right\} v(p_+)$$

$$M_{2V} + M_{4V} + \left(M_{12V}\right)_{rem} =$$

$$= -\frac{\alpha^2}{q^2} \ln \frac{\Lambda^2}{m^2} \bar{u}(p_-) \left\{ \epsilon\cdot\gamma \frac{1}{p_-\cdot\gamma - k\cdot\gamma - m} a\cdot\gamma \right\} v(p_+) \qquad (20)$$

$$M_{9V} = \frac{\alpha^2}{q^2} \ln \frac{\Lambda^2}{m^2} \bar{u}(p_-) \left\{ a\cdot\gamma \frac{1}{-p_+\cdot\gamma + k\cdot\gamma - m} \epsilon\cdot\gamma \right\} v(p_+)$$

$$- \frac{\alpha^2}{q^2} \ln \left(\frac{2k\cdot p_+}{m^2} \right) \bar{u}(p_-) \left\{ a\cdot\gamma \frac{1}{-p_+\cdot\gamma + k\cdot\gamma - m} \epsilon\cdot\gamma \right\} v(p_+)$$

$$M_{10V} = \frac{\alpha^2}{q^2} \ln \frac{\Lambda^2}{m^2} \bar{u}(p_-) \left\{ \epsilon\cdot\gamma \frac{1}{p_-\cdot\gamma - k\cdot\gamma - m} a\cdot\gamma \right\} v(p_+)$$

$$M_{13V} = 0$$

$$M_{14V} = 0$$

The terms

$$\bar{u}(p_-)\,\frac{a\cdot\gamma\ k\cdot\gamma\ \epsilon\cdot\gamma}{(-2k\cdot p_+)}\,v(p_+)$$

and

$$\bar{u}(p_-)\,\frac{a\cdot\gamma\ p_-\cdot\gamma\ \epsilon\cdot\gamma}{(-2k\cdot p_+)}\,v(p_+)$$

may be replaced by

$$\bar{u}(p_-)\left\{a\cdot\gamma\,\frac{1}{-p_+\cdot\gamma + k\cdot\gamma - m}\,\epsilon\cdot\gamma + \epsilon\cdot\gamma\,\frac{1}{p_-\cdot\gamma - k\cdot\gamma - m}\,a\cdot\gamma\right\}v(p_+)\quad,$$

introducing errors of order m/k. We may thus write the non-infrared virtual photon radiative correction matrix element as

$$M_V = \frac{-4\pi\alpha}{q^2}\,\bar{u}(p_-)\left\{a\cdot\gamma\,\frac{1}{-p_+\cdot\gamma + k\cdot\gamma - m}\,\epsilon\cdot\gamma + \epsilon\cdot\gamma\,\frac{1}{p_-\cdot\gamma - k\cdot\gamma - m}\,a\cdot\gamma\right\}v(p_+)\times \tag{21}$$

$$\times\left(\frac{\alpha}{4\pi}\right)\left\{\left[\frac{3(2p_+\cdot p_-)}{(2k\cdot p_+)} - \frac{1}{2}\right]\ln\left(\frac{2p_+\cdot p_-}{m^2}\right) - \frac{1}{2}\ln\left(\frac{2k\cdot p_+}{m^2}\right)\right\}\quad.$$

The lowest order radiative correction resulting from the non-infrared virtual photons is given by the interference of M_V with $M_{B\text{-}H}$. One obtains

$$\sigma(\text{virtual}) = \frac{\alpha}{4\pi}\left\{\left[\frac{6(2p_+\cdot p_-)}{(2k\cdot p_+)} - 1\right]\ln\left(\frac{2p_+\cdot p_-}{m^2}\right) - \ln\left(\frac{2k\cdot p_+}{m^2}\right)\right\}\ \sigma_{B\text{-}H}\quad. \tag{22}$$

C. Real Photon Terms

The remaining real photon matrix elements were calculated by combining the non-infrared parts of diagrams 1R, 3R, 4R, and 6R with diagrams 2R and 5R into two matrix elements, each of which was gauge invariant in both photons. The non-infrared real photon radiative corrections were found to be[6]

$$\sigma(\text{real}) = \frac{4\alpha^4}{\pi^2} \ln\left(\frac{2\omega_-}{m}\right) \frac{1}{k^2 m^4} \left\{\frac{1}{6}(k-\omega_- -m)^3 + m(k-\omega_-)(k-\omega_- -m)\right\} \qquad (23)$$

after integrating over the appropriate final phase space for both the unobserved positive muon and the soft photon.

In addition to the terms mentioned above, several terms of order $\alpha \ln^2(\omega_-/m)\sigma_{B-H}$ appeared in both virtual and real radiative cross sections but cancelled out of the total radiative correction. The total radiative correction is the sum of Eqs. (19), (22), and (23).

IV. COMPTON CORRECTIONS

Besides the Bethe-Heitler process for producing muon pairs, it is possible that the incident photon can be scattered by a virtual Compton process with the resulting time-like photon decaying into a $\mu^+ - \mu^-$ pair. If the invariant mass of the final muon pair is close to that of a heavy photon resonance (e.g. ρ^o or ω), we expect an enhancement of the cross section for muon pair production at that energy. If the μ^- is detected at small angles ($\theta_- \lesssim m/k$) and with essentially all of the incident photon energy, the invariant mass of the final muon pair is $\approx (2km)^{1/2}$. Therefore, we expect this process to be most significant for $k \approx m_v^2/2m$.

In the following sections we calculate the production of muon pairs via vector resonance channels. In (A) the vector resonance is produced by a one-pion-exchange (OPE) model and in (B) a diffraction model is used.

A. One-Pion-Exchange

Let us assume the incident photon is coupled to the vector resonance and the nucleon as shown in Fig. 4.[7] The $\gamma\pi v_1$ vertex has a unique (up to a form factor) gauge invariant form of

$$\frac{f_{\gamma\pi v_1}}{m_\pi} \epsilon_{abcd}\, \epsilon^a(\gamma)\, k^b(\gamma)\, \epsilon^c(v_1)\, k^d(v_1) \ . \tag{24}$$

With this vertex, the coupling constant is normalized to the partial

width of the process $v_1 \to \gamma + \pi$.

$$\Gamma_{v_1 \to \gamma\pi} = \frac{1}{24}\left(\frac{f^2_{\gamma\pi v_1}}{4\pi}\right)\frac{m^3_{v_1}}{m^2_\pi}\left[1 + O\left(\frac{m^2_\pi}{m^2_{v_1}}\right)\right] \tag{25}$$

We also assume that the vector resonance couples to photons with the coupling

$$\frac{e}{2\gamma_{v_1}} m^2_{v_1} \underset{\sim}{\epsilon}(\gamma) \cdot \underset{\sim}{\epsilon}(v_1) \quad . \tag{26}$$

The inverse coupling constant $1/2\ \gamma_{v_1}$ is related to the leptonic decay width of the vector resonance by

$$\Gamma_{v_1 \to \mu^+\mu^-} = \frac{\alpha^2}{(\gamma^2_{v_1}/4\pi)}\frac{m_{v_1}}{12}\left[1 + O\left(\frac{m^4_\mu}{m^4_{v_1}}\right)\right] \quad . \tag{27}$$

Near resonance ($k \approx m^2_{v_1}/2m$) and for $\theta_- \to 0$, and $\omega_- \to k$, the cross section as calculated with the OPE model is

$$\frac{d^2\sigma}{d\Omega_- d\omega_-} = \frac{9}{4}\left(\frac{\Gamma_{v_1 \to \pi\gamma}}{\Gamma_{v_1}}\right)\left(\frac{g^2_{\pi N}}{4\pi}\right)\left(\frac{\Gamma_{v_1 \to \mu^+\mu^-}}{m_{v_1}}\right)\frac{1}{mM^2}\cdot\frac{1}{(1 + m^2_\pi/m^2)^2} \tag{28}$$

where $g^2_{\pi N}/4\pi = 14$ is the nucleon coupling constant.

B. Diffraction

The present data on the photoproduction of vector resonances such as the ρ^o seems to be inconsistent with the OPE model while a

diffraction model seems much more consistent.[8] In order to estimate the cross section for muon pairs in a diffraction model, we use the Amati, Fubini, Stanghellini[9] model of diffraction scattering to relate the vector resonance photoproduction to observed π-N diffraction measurements. Using this model, we replace the top rung of a ladder graph for π-N diffraction with a γ-v rung as in Fig. 5.

The $v_1 \pi v_2$ vertex has a unique gauge invariant form of

$$\frac{f_{v_1 \pi v_2}}{m_\pi} \epsilon_{abcd} \epsilon^a(v_1) k^b(v_1) \epsilon^c(v_2) k^d(v_2) . \tag{29}$$

In Ref. 7, the top rung of Fig. 5(b) was approximated by

$$\frac{f_{\gamma\pi\omega} f_{\rho\pi\omega}}{m_\pi^2} \left(\underset{\sim}{\epsilon}(\rho) \cdot \underset{\sim}{\epsilon}(\gamma)\right) \left[\frac{1}{4} m_\rho^4\right] , \tag{30}$$

with $v_1 = \omega$, $v_2 = \rho$, and $m_{v_1} = m_{v_2} = m_\rho$. Under similar conditions but with arbitrary vector mesons (note that the G parity of v_1 and v_2 must be different), this rung can be approximated by

$$\frac{f_{\gamma\pi v_1} f_{v_1 \pi v_2}}{m_\pi^2} \left(\underset{\sim}{\epsilon}(v_1) \cdot \underset{\sim}{\epsilon}(\gamma)\right) \frac{1}{4} \left[m_{v_1}^2 m_{v_2}^2 + m_{v_1}^4 - m_{v_2}^4\right] . \tag{31}$$

The top rung of Fig. 5(a) can be approximated in the forward direction by

$$g_{v_3 \pi\pi}^2 m_{v_3}^2 \left[1 + O\left(m_\pi^2/m_{v_3}^2\right)\right] \tag{32}$$

where

$$\Gamma_{v_3 \to \pi\pi} = \frac{1}{12}\left(\frac{g^2_{v_3\pi\pi}}{4\pi}\right)\left\{1 - \frac{4m_\pi^2}{m^2_{v_3}}\right\}^{3/2} m_{v_3} \quad . \tag{33}$$

Using Eqs. (31) and (32), we may relate muon pair production through a diffraction process to the total π-nucleon diffraction scattering cross section by

$$\frac{d^2\sigma}{d\Omega_- d\omega_-} = \frac{9}{4(4\pi)^2}\left(\frac{\Gamma_{v_1 \to \pi\gamma}}{\Gamma_{v_2}}\right)\left(\frac{\Gamma_{v_2 \to \mu^+\mu^-}}{m_{v_2}}\right)\left(\frac{m_{v_3}}{12\Gamma_{v_3}}\right)^2 \times$$
$$\times \left(\frac{mk^2\,\sigma^{T^2}_{\pi N}(k)}{m_{v_1}\, m_{v_2}}\right)\left(\frac{f^2_{v_1\pi v_2}}{4\pi}\right)\frac{\left(m^2_{v_1}\, m^2_{v_2} + m^4_{v_1} - m^4_{v_2}\right)^2}{\left(m^2_\pi\, m^2_{v_1}\, m^4_{v_3}\right)} \quad . \tag{34}$$

At present, the most likely candidates for the vector resonances are $v_1 = \rho$, $v_2 = \omega$, and $v_3 = \rho$. Since $m_\rho \approx m_\omega \approx 780$ MeV, the resonance photon energy is approximately 2.9 GeV. At this energy, using $\Gamma_{\rho\pi\gamma} \approx 0.15$ MeV, $\Gamma_{\omega \to \mu^+\mu^-} \approx 10^{-4}\,\Gamma_\omega$, $f^2_{\omega\pi\rho}/4\pi \approx 0.4$, and $\sigma_{\pi N} \approx 27$ mb, the contribution of the diffraction channel is about one percent of the Bethe-Heitler cross section.

V. PION BACKGROUND

Another possible source of high energy muons is through the reactions

$$\gamma + p \rightarrow \pi^- + (\text{anything})$$
$$\qquad\qquad\quad \hookrightarrow \mu^- + \bar{\nu}_\mu \ .$$

There are several possible processes by which it is possible to photoproduce a high energy π^-. The two most likely candidates are peripheral one-pion-exchange as in Fig. 6(a) and diffraction production of a ρ^o with its subsequent decay into a $\pi^+ \pi^-$ pair as in Fig. 6(b).

The cross section for producing negative pions at energy $\omega_- \gg m_\pi$ and angle $\theta_- \lesssim m_\pi/\omega_-$ via a peripheral one-pion-exchange mechanism was shown by Drell[10] to be

$$\frac{d^2\sigma}{d\Omega_- d\omega_-} = \frac{\alpha}{8\pi^2} \frac{\sin^2 \theta_-}{(1 - \beta_- \cos \theta_-)^2} \frac{\omega_-(k - \omega_-)}{k^3} \sigma^T_{\pi^+ p}(k - \omega_-) \ . \qquad (35)$$

This formula assumes $k - \omega_- \gg m_\pi$ so that the velocity of the π^+ in the scattering $\pi^+ + p \rightarrow \pi^+ + p$ is near unity. To correct for this, we multiply $\sigma^T_{\pi^+ p}$ by

$$\underset{\sim}{v} = \left((k - \omega_-)^2 - m_\pi^2\right)^{1/2}/(k - \omega_-) \ .$$

Thus, near threshold, the cross section is

$$\frac{d^2\sigma}{d\Omega_- d\omega_-} = \frac{\alpha}{8\pi^2} \frac{\sin^2\theta_-}{(1 - \beta_- \cos\theta_-)^2} \frac{\omega_- \left[(k-\omega_-)^2 - m_\pi^2\right]^{1/2}}{k^3} \sigma^T_{\pi^+ p}(k-\omega_-). \qquad (36)$$

This formula reduces to Drell's original formula for $k - \omega_- \gg m_\pi$.

Muons from the decay of these photoproduced pions could enter the detection apparatus of an experiment and would be indistinguishable from muons from the Bethe-Heitler process. The difference in the threshold energy for muons and for pions is approximately 40 MeV. If the energy resolution of the detection apparatus is restricted to this 40 MeV region, muons from pion decay are kinematically forbidden. As one goes below the threshold for pions, the cross section in Eq. (36) quickly becomes larger than the Bethe-Heitler cross section. The pion cross section is especially large in the region of the 3,3 resonance for the $\pi^+ p$ system. If the energy resolution of the detection apparatus is too large, the number of spurious muons will be an appreciable fraction of the number of Bethe-Heitler muons. Thus, the presence of muons from pion decay puts an upper limit on the energy resolution of an experiment.

The pion flux from ρ° decay can be calculated as follows. The present experimental data on ρ° photoproduction indicates that there is a sharp diffraction peak in the forward direction. In

fact, the cross section can be written as[8]

$$\left(\frac{d\sigma}{d\Omega}\right)_{\gamma\rho} = \left(\frac{d\sigma}{d\Omega}\,(0^\circ)\right)_{\gamma\rho} e^{Bt} \quad ,$$

where t is the invariant momentum transfer $t = (k - p_\rho)^2$ and $B \approx 9.5\ (\mathrm{BeV/c})^{-2}$. If this ρ° then decays into a pion pair with the negative pion produced at small angles and with all except a few hundred MeV of the available energy, t will be near its minimum value $t_{min} \approx -(m_\rho^2/2k)^2$. We may then approximate the ρ° production cross section by its value at 0°. The error is this approximation is in overestimating the pion flux. We then let the ρ° propagate to the $\rho\pi\pi$ vertex with a propagator

$$\left[(p_+ + p_-)^2 - m_\rho^2 + i m_\rho \Gamma_\rho\right]^{-1} .$$

The pion decay vertex is given by $g_{\rho\pi\pi}\,(p_- - p_+)_\mu$.

After integration over the phase space available to the π^+ consistent with the ρ° propagator, we find

$$\frac{d^2\sigma}{d\Omega_- d\omega_-} \approx \left(\frac{d\sigma}{d\Omega}(0^\circ)\right)_{\gamma\rho} \frac{3}{2\pi} \frac{p_-^2 \sin^2\theta_-}{m_\rho^2 k} \times$$

$$\times \left[\tan^{-1} \frac{4\omega_+\omega_- - m_\rho^2 + 2m_\pi^2}{m_\rho \Gamma_\rho} + \tan^{-1} \frac{m_\rho^2 - 2\omega_+\omega_-(1-\beta_+) - 2m_\pi^2}{m_\rho \Gamma_p}\right] \qquad (37)$$

for $\theta_- \lesssim m_\pi/k$ and $k - \omega_- \approx 1 - 4m_\pi$.

For $k \approx 15$ GeV, $\theta_- \lesssim m_\pi/k$, and $k - \omega_- \lesssim 4m_\pi$, this cross section is smaller than that of the peripheral model discussed above by at least an order of magnitude. At energies and angles larger than these, the ρ^o decay process is even more negligible.

As an example of how the pion background limits the energy resolution of an experiment, let us consider an experiment at $k = 15$ GeV and $\theta_- = 0.2^o$. The cross sections for π^- photoproduction [Eq. (36)] and for μ^- photoproduction [Eq. (10)] are plotted in Fig. 7.

At 15 GeV, a π^- will travel approximately 800 meters before it decays into a μ^- (assuming a lifetime of 2.5×10^{-8} sec.). Since the detection apparatus is unlikely to be more than ten per cent of this decay distance from the target, only a few per cent of the photoproduced pions will decay in time for the decay muon to enter the detector. It is relatively easy to discriminate between pions and muons at the detector.

As one can see from Fig. 7, the pion cross section is an order of magnitude larger than the muon cross section for $\omega_- \approx 14.66$ GeV. Thus, if the energy resolution of the detector extends from threshold ($\omega_- \approx 14.88$ GeV) to the region of the peak in the π^- cross section, at least several per cent of the muons which are detected will come from π^- decay. If the energy resolution is restricted to approximately 100 MeV below threshold, only about one per cent of the muons will be from π^- decay.

Thus, in order to do an accurate experiment, the energy resolution must be large enough to obtain a resonable counting rate and small enough to limit the number of muons from pion decay.

VI. CONCLUSION

In this paper we have analyzed a proposal for a new experimental test of muon quantum electrodynamics. Such an experiment is now being conducted at the Stanford HEPL electron linac at 800 MeV[11] and another experiment is being planned for SLAC at 15-20 GeV.[12]

An expression for the pair-production cross section has been derived and the radiative corrections estimated. The effect of virtual Compton processes has been shown to be negligible at the energies of interest to the two experiments above. The spurious background of muons from the decay of pions has been shown to limit the energy resolution of an experimental test of the theory.

The 800 MeV experiment will test the validity of the quantum electrodynamic description of the muon propagator at virtual muon masses of $\approx$ 400 MeV while the 20 GeV experiment will test the propagator at $\approx$ 2 GeV.

It may also be possible to probe for new vector resonances with mass $\approx (2km)^{1/2}$ by varying the photon energy and detecting the muon decay mode of these resonances.

ACKNOWLEDGMENT

The writer wishes to thank Professor S. D. Drell for suggesting this problem and for advising him throughout the calculation.

Table I. Glossary of Symbols

k	4-momentum of incident γ-ray = $(k_o, \underset{\sim}{k})$
p_-	4-momentum of outgoing negative muon = $(\omega_-, \underset{\sim}{p}_-)$
p_+	4-momentum of outgoing positive muon = $(\omega_+, \underset{\sim}{p}_+)$
P	4-momentum of initial proton = $(M, \underset{\sim}{0})$
P'	4-momentum of recoil proton = $(E', \underset{\sim}{P}')$
q	$P - P' = p_+ + p_- - k$
z	$p_- - k$
ϵ	polarization 4-vector of incident γ-ray
a_μ	proton matrix element = $- ie \cdot \bar{u}(P') \gamma_\mu u(P)$
m	mass of muon
M	mass of proton
θ_-	angle between $\underset{\sim}{p}_-$ and $\underset{\sim}{k}$ in laboratory
Λ	large regulator mass in radiative corrections
λ	photon mass (for handling infrared divergences)
α	$e^2/4\pi \approx 1/137$
μ	proton magnetic moment (2.79 nuclear magnetons)

REFERENCES

1. For a general treatment of quantum electrodynamics see, for example, J. D. Bjorken and S. D. Drell, Relativistic Quantum Mechanics and Relativistic Quantum Fields (McGraw-Hill Book Company, Inc., New York, 1964 and 1965). Our notation will follow that of the above. In particular $\hbar = c = 1$, $e^2/4\pi \equiv \alpha \approx 1/137$, $p_\mu \gamma^\mu \equiv p \cdot \gamma$. For a recent review of the status of quantum electrodynamics, see F. M. Pipkin, Proceedings of the Oxford International Conference on Elementary Particles, Sept. 1965.

2. R. B. Blumenthal, D. C. Ehn, W. L. Faissler, P. M. Joseph, L. J. Lanzerotti, F. M. Pipkin, and D. G. Stairs, Phys. Rev. Letters 14, 660 (1965). E. Eisenhandler, J. Feigenbaum, N. B. Mistry, P. J. Mostek, D. R. Rust, A. Silverman, C. K. Sinclair, and R. M. Talman, Bull. Am. Phys. Soc. 11, 20 (1966).

3. S. D. Drell, Phys. Rev. Letters 13, 257 (1964).

4. S. D. Drell and J. D. Walecka, Ann. Phys. (N.Y.) 28, 18 (1964). Note that our metric is different from that of this reference.

5. D. R. Yennie, S. C. Frautschi, and H. Suura, Ann. Phys. (N.Y.) 13, 379 (1961).

6. Some of the longer traces from the real photon matrix elements were taken with the aid of "FTRACE". See S. M. Swanson, "FTRACE: A FAP Subroutine for Dirac Gamma Matrix Algebra," Stanford preprint ITP-120 (unpublished).

7. S. M. Berman and S. D. Drell, Phys. Rev. 133, B791 (1964).

8. L. J. Lanzerotti, R. B. Blumenthal, D. C. Ehn, W. L. Faissler, P. M. Joseph, F. M. Pipkin, J. K. Randolph, J. J. Russell, D. G. Stairs, and J. Tenenbaum, Phys. Rev. Letters 15, 210 (1965).

9. D. Amati, S. Fubini, and A. Stanghellini, Nuovo Cimento 26, 896 (1962).

10. S. D. Drell, Phys. Rev. Letters 5, 278 (1960).

11. D. Quinn (private communication).

12. L. Mo (private communication).

FIGURE CAPTIONS

1. "Bethe-Heitler" diagrams for pair production.
2. Feynman diagrams for virtual photon radiative corrections.
3. Feynman diagrams for real photon radiative corrections.
4. One-pion-exchange production of muon pairs.
5. Rung diagrams for diffraction scattering:
   (a) Pion-nucleon
   (b) Photoproduction of vector resonances.
6. Pion background diagrams:
   (a) One-pion-exchange contribution to π^- production
   (b) Diffraction production of a ρ^o with its subsequent decay into a pion pair.
7. Muon and pion photoproduction cross sections at $k = 15$ GeV and $\theta_- = 0.2^o$.

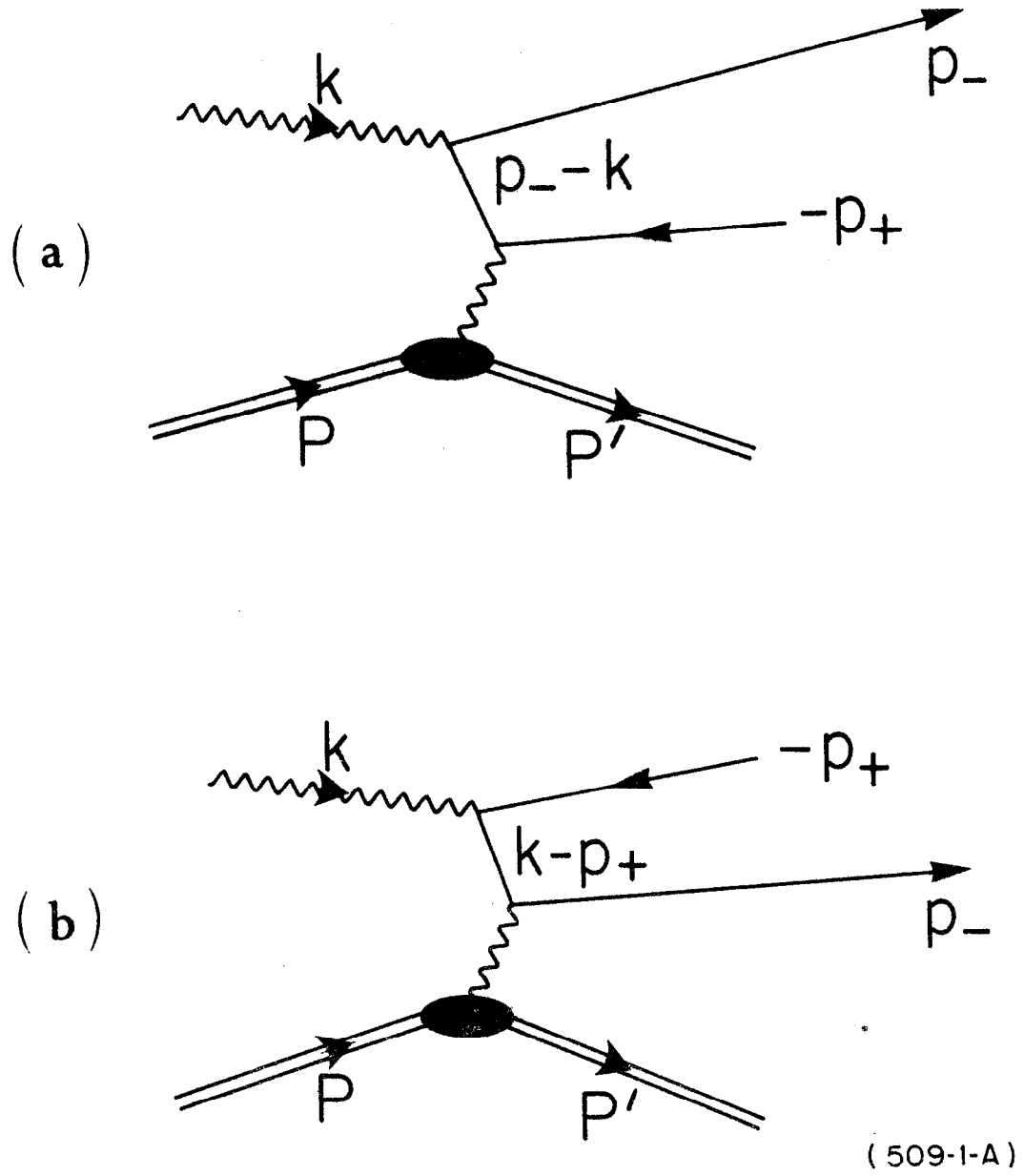

Fig. 1

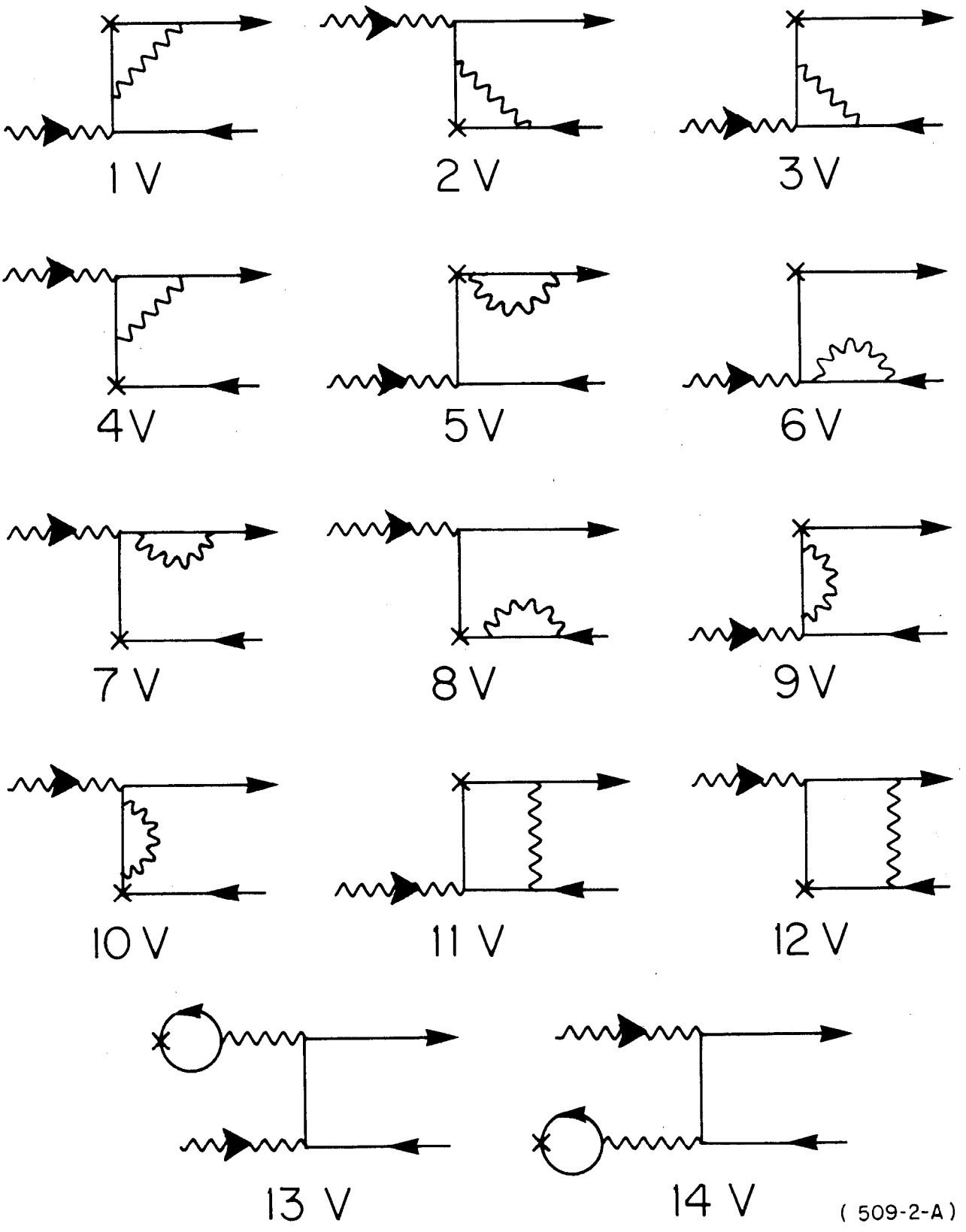

Fig. 2

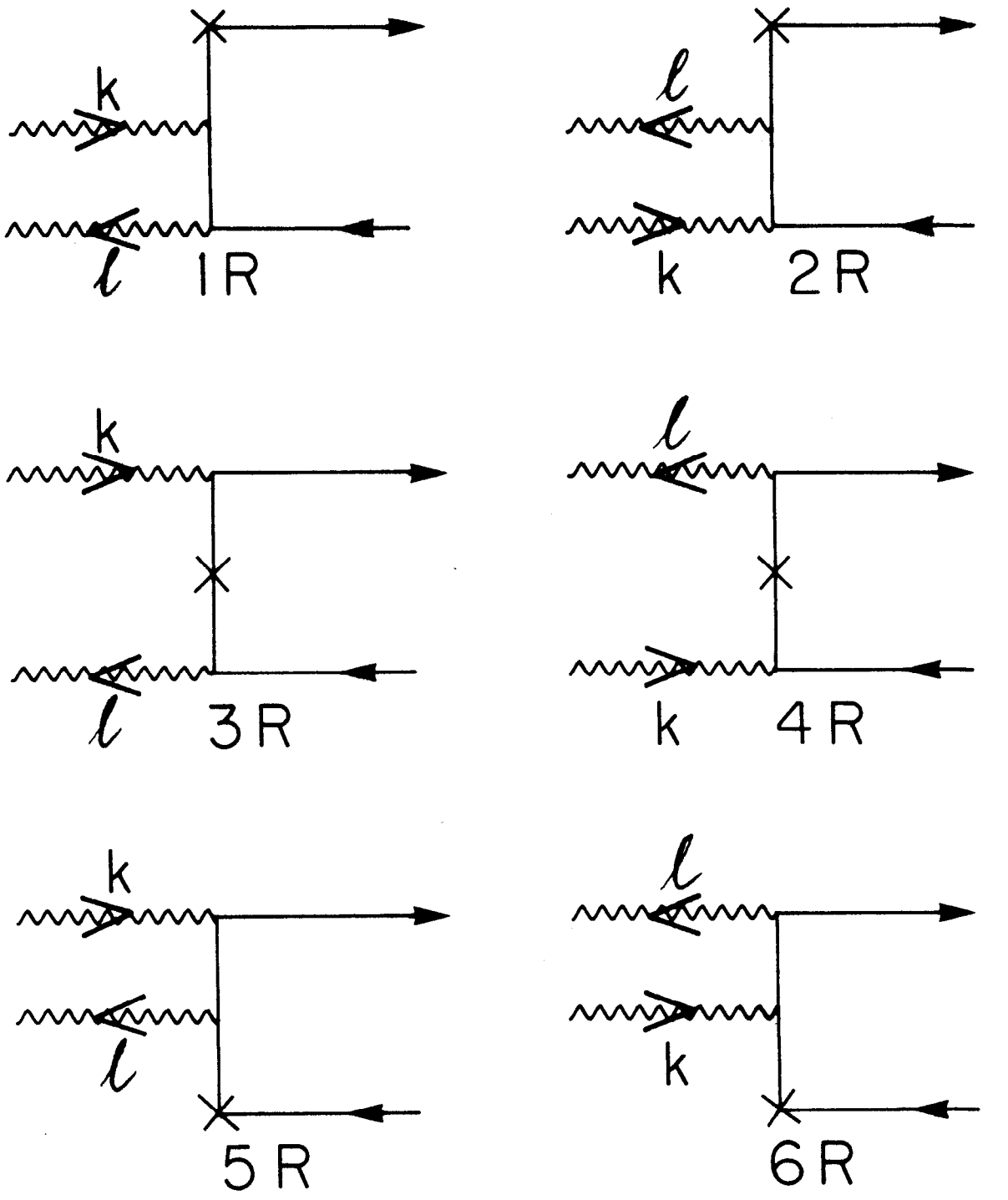

Fig. 3

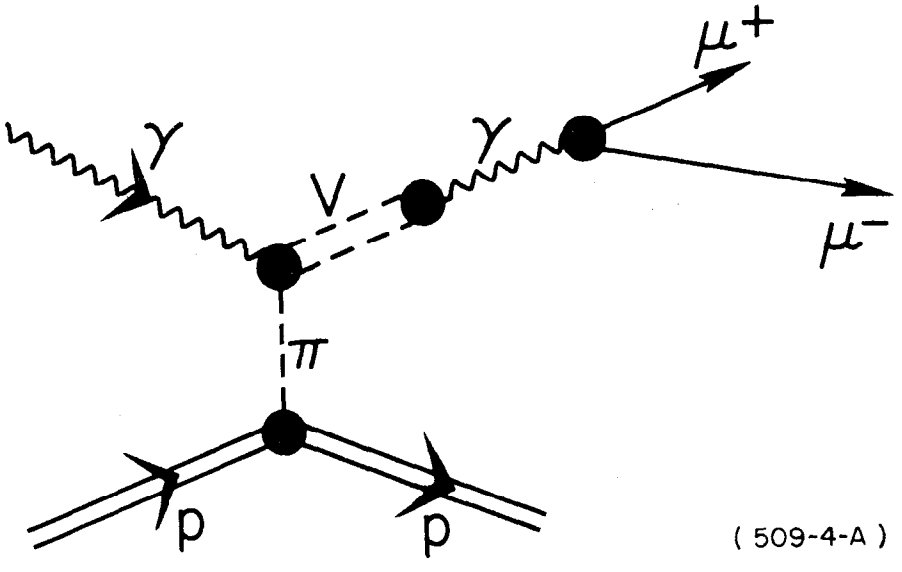

Fig. 4

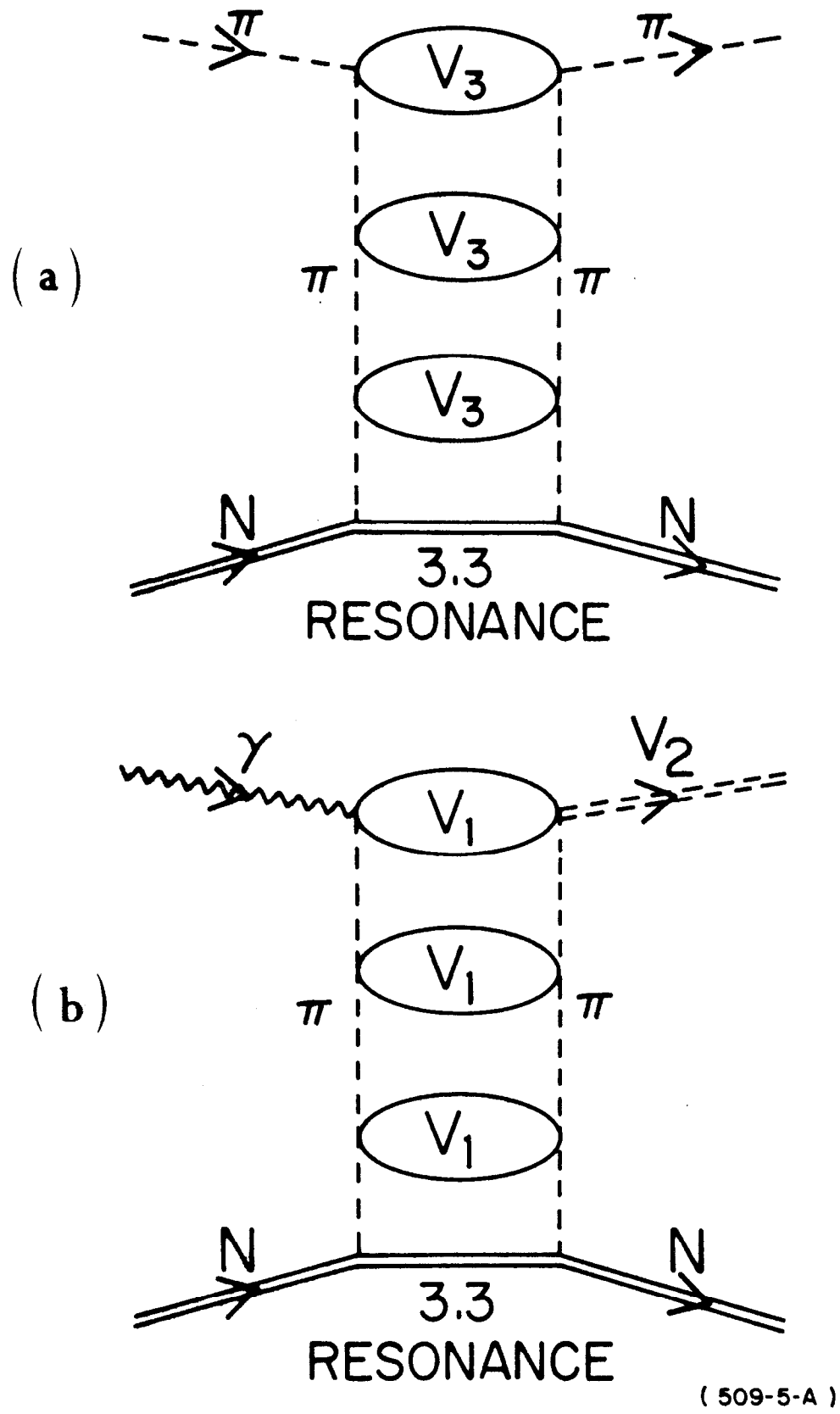
(a)
π
π
V3
V3
V3
π
π
N
N
3.3
RESONANCE
(b)
γ
V2
V1
V1
V1
π
π
N
N
3.3
RESONANCE
(509-5-A)

Fig. 5

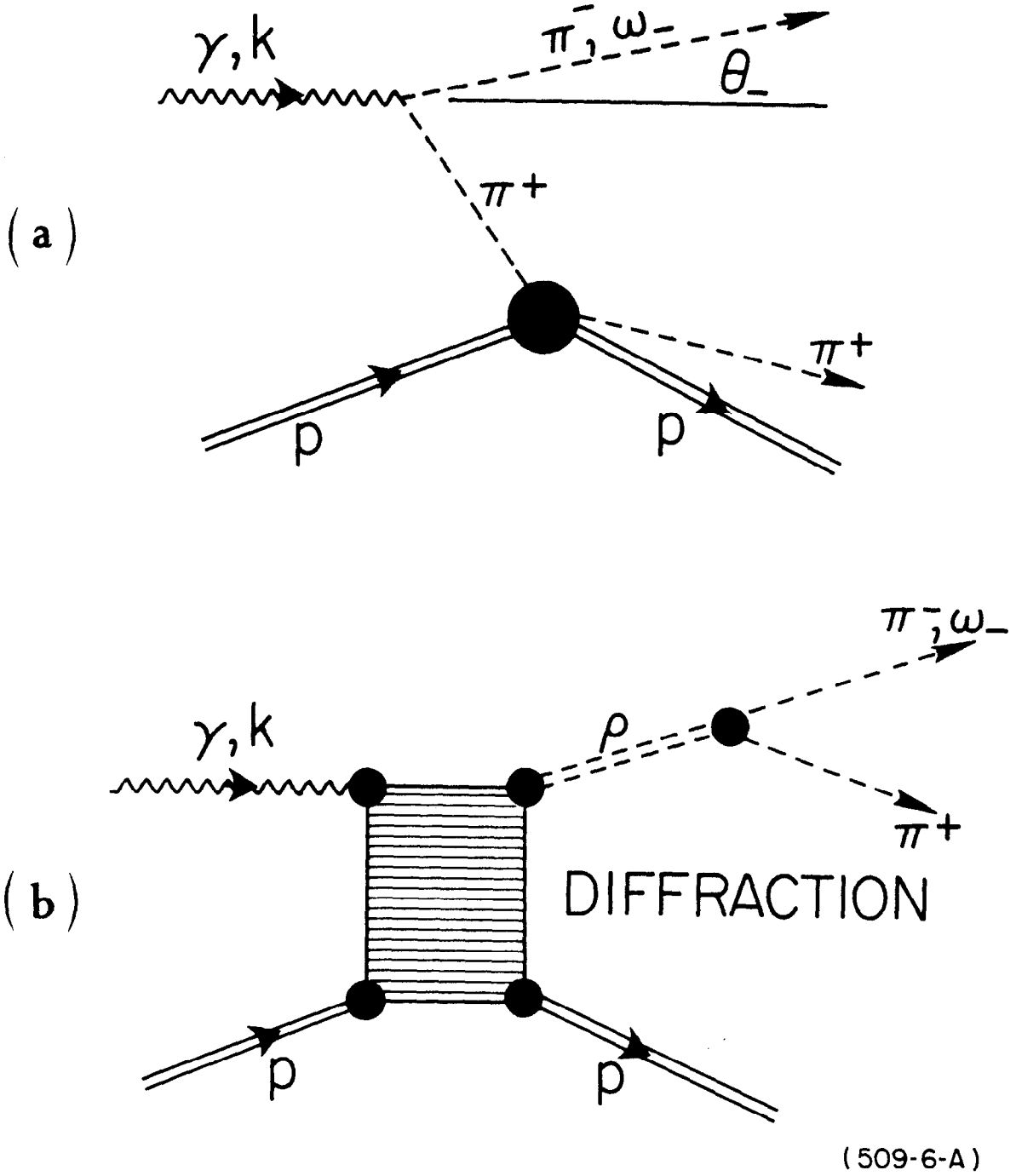

Fig. 6

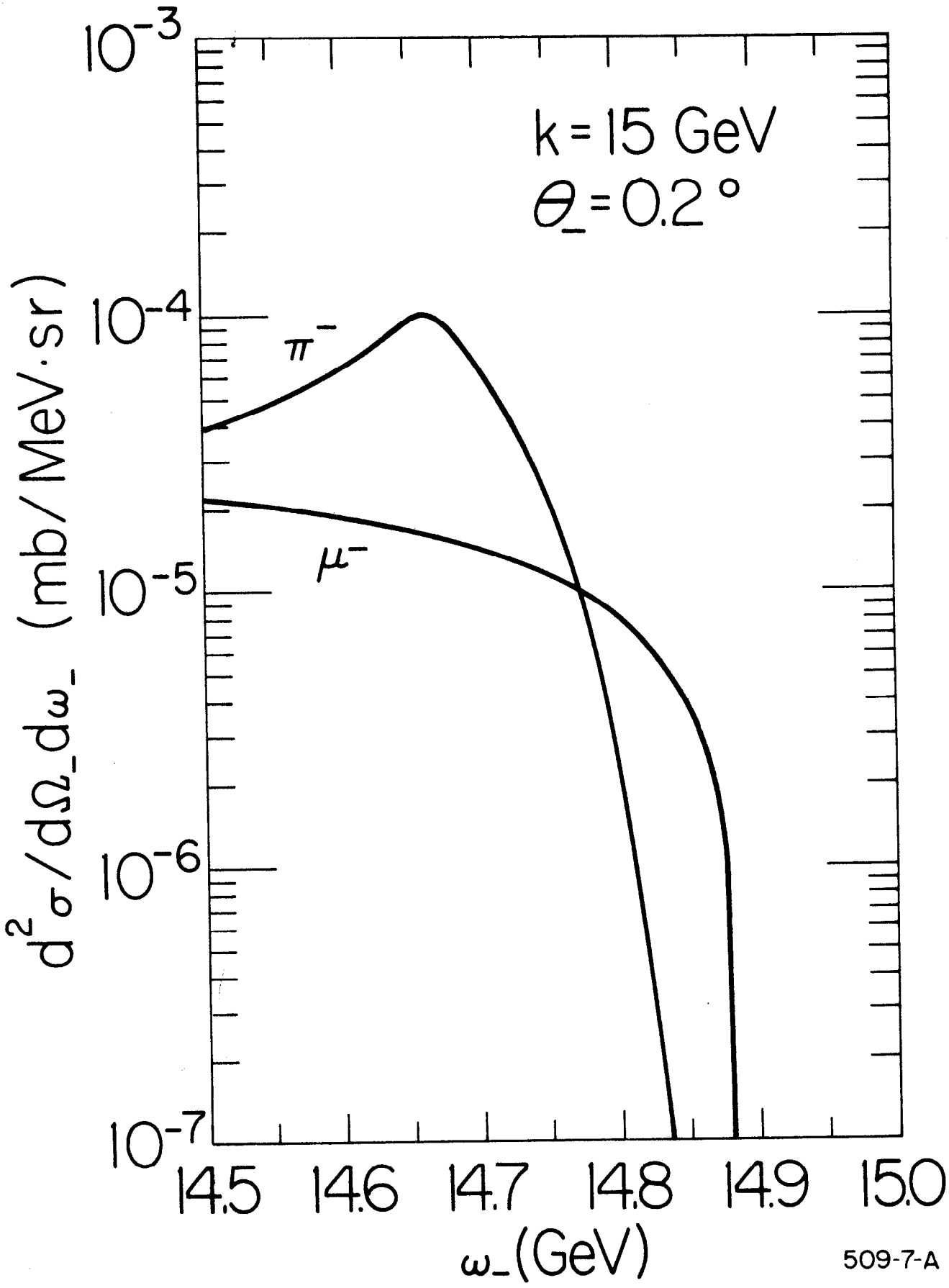
k = 15 GeV
θ_ = 0.2°
π⁻
μ⁻
10⁻³
10⁻⁴
10⁻⁵
10⁻⁶
10⁻⁷
d²σ/dΩ_dω_ (mb/MeV·sr)
14.5
14.6
14.7
14.8
14.9
15.0
ω_(GeV)
509-7-A

Fig. 7